

Prototyping of MODIS LAI and FPAR Algorithm with LASUR and LANDSAT Data

Yuhong Tian, Yu Zhang, Yuri Knyazikhin, Ranga B. Myneni, Joseph M. Glassy, Gerard Dedieu, and Steven W. Running

Abstract—This paper describes results from prototyping of the moderate resolution imaging spectroradiometer (MODIS) radiative transfer-based synergistic algorithm for the estimation of global leaf area index (LAI) and fraction of photosynthetically active radiation (FPAR) absorbed by vegetation using land surface reflectances (LASUR) and Landsat data. The algorithm uses multispectral surface reflectances and a land cover classification map as input data to retrieve global LAI and FPAR fields. Our objectives are to evaluate its performance as a function of spatial resolution and uncertainties in surface reflectances and the land cover map. We analyzed reasons the algorithm can or cannot retrieve a value of LAI/FPAR from the reflectance data and justified the use of more complex algorithms, instead of NDVI-based methods. The algorithm was tested to investigate the effects of vegetation misclassification on LAI/FPAR retrievals. Misclassification between distinct biomes can fatally impact the quality of the retrieval, while the impact of misclassification between spectrally similar biomes is negligible. Comparisons of results from the coarse and fine resolution retrievals show that the algorithm is dependent on the spatial resolution of the data. By evaluating the data density distribution function, we can adjust the algorithm for data resolution and utilize the algorithm with data from other sensors.

Index Terms—Fraction of photosynthetically active radiation (FPAR), land surface reflectances (LASUR), LANDSAT, leaf area index (LAI), moderate resolution imaging spectroradiometer (MODIS).

I. INTRODUCTION

THE importance of vegetation in studies of global climate and biogeochemical cycles is well recognized [1]. Presently, most ecosystem productivity models, carbon budget models, and global models of climate, hydrology and biogeochemistry require vegetation parameters to calculate land surface photosynthesis, evapotranspiration and net primary production [2]–[6]. Therefore, accurate estimates of vegetation parameters are increasingly important in the carbon cycle, the energy balance and environmental impact assessment studies. Two of these parameters are green leaf area index (LAI), a canopy structural variable, and fraction of photosynthetically

active radiation (0.4–0.7 μm) absorbed by vegetation (FPAR), a radiometric variable. In order to quantitatively and accurately model global vegetation dynamics and differentiate short-term from long-term trends, as well as to distinguish regional from global phenomena, these two parameters must be collected often for a long period of time and should represent every region of the Earth's lands [7].

These two parameters are estimated from remote sensing data using empirical relationships between values of LAI/FPAR and vegetation indices which include near-infrared (NIR) to red (RED) band ratios and the normalized difference vegetation index (NDVI) [9]–[15]. The limitations of such methods are well known [16]–[18]. No unique relationship between LAI/FPAR and vegetation index is applicable everywhere and all the time [19]–[21] because the reflectances of plant canopies depend on a number of other factors, such as, measurement geometry and spatial resolution. These empirical relationships are site- and sensor-specific, and are unsuitable for application to large areas or in different seasons [19]. A physically based model to describe the propagation of light in plant canopies and its use in retrieval of biophysical parameters is the preferred alternative. In the context of the Earth Observing System (EOS), the land discipline group of the moderate resolution imaging spectroradiometer (MODIS) Science Team is developing algorithms for the determination of landcover, LAI, albedo, etc. to be operationally generated from data from one or more of satellites [22].

One of these algorithms is the synergistic algorithm for the estimation of global LAI/FPAR from MODIS [7]. At the present time, the algorithm has been developed and theoretically justified, but no evidence of its functionality has been presented. The purpose of this paper is to evaluate the physical functionality and performance of the algorithm by prototyping with the land surface reflectances (LASUR) data derived from the advanced very high resolution radiometer (AVHRR) data and Landsat data. Specifically, we would like to know: What is the effect of uncertainties in surface reflectances on the quality of retrieved LAI/FPAR? When and why the algorithm does/does not retrieve a value of LAI/FPAR from the reflectance data? How can an assessment of the algorithm accuracy be made? What is the behavior of the algorithm as a function of spatial resolution? In this paper, first we describe the concepts of the algorithm, the physical meaning of the bidirectional reflectance distribution functions (BRDF) equation, and the method to adjust the look-up table (LUT). Then the spectral signatures of LASUR and Landsat were analyzed, followed by a series of algorithm prototyping results discussed in the later section.

Manuscript received June 1, 1999; revised March 1, 2000. This work was supported by the National Aeronautics and Space Administration through MODIS Contract NAS5-96061.

Y. Tian, Y. Zhang, Y. Knyazikhin, and R. B. Myneni are with the Department of Geography, Boston University, Boston, MA 02215 USA (e-mail: ytian@crsa.bu.edu).

J. M. Glassy and S. W. Running are with the School of Forestry, University of Montana, Missoula, MT 59812 USA.

G. Dedieu is with CESBIO-Unite mixte CNES-CNRS-UPS, Toulouse, France.

Publisher Item Identifier S 0196-2892(00)06226-4.

Results from prototyping are a valuable means of testing the physics of the algorithm and also constitute an important first step toward improving the algorithm. At the most general level, this research contributes to an improved understanding of the algorithm behavior. A more practical benefit is to provide a basis for improved retrieval of surface parameters from satellite data.

II. ALGORITHM

A. Statement of the Problem

The inverse problem of retrieving LAI and FPAR from atmospherically corrected BRDF is formulated as follows. Given sun Ω_0 and view Ω_v directions, vegetation type, BRDF's d_k ($k = 1, 2, \dots, N$) at N spectral bands and their uncertainties δ_k ($k = 1, 2, \dots, N$), find LAI and FPAR. The retrievals are performed by comparing observed and modeled BRDF's for a suite of canopy structures and soil patterns that cover a range of expected natural conditions. All canopy/soil patterns for which the magnitude of residuals in the comparison does not exceed uncertainties in observed and modeled BRDF's, i.e.,

$$\frac{1}{N} \sum_{k=1}^N \left(\frac{\mathbf{r}_k(\Omega_v, \Omega_0, p) - d_k}{\delta_k} \right)^2 \leq 1 \quad (1)$$

are treated as acceptable solutions to the inverse problem. Here $\mathbf{r}_k(\Omega_v, \Omega_0, p)$, $k = 1, 2, \dots, N$, are modeled BRDF's, and $p = [\text{canopy, soil}]$ denotes a canopy/soil pattern, which is unknown and will be discussed later. For each acceptable solution, a value of FPAR is also evaluated. Mean values of LAI and FPAR averaged over the set of acceptable solutions are taken as solutions of the inverse problem. A mathematical justification of this procedure is presented in [7]. Its application to the retrieval of LAI and FPAR from multi-angular observation is discussed in [23].

B. Radiation Transport in a Canopy

For MODIS LAI/FPAR algorithm, a three-dimensional (3-D) radiative transfer model is used to derive spectral and angular biome-specific signatures of vegetation canopies. Taking into account features specific to the problem of radiative transfer in plant canopies, powerful techniques developed in nuclear physics were utilized to split a complicated 3-D radiative transfer problem into two independent, simpler subproblems. The first subproblem describes the radiative regime within the vegetation canopy for the case of a black surface underneath the medium ("black soil problem"). The second subproblem is the radiation field in the vegetation canopy generated by anisotropic heterogeneous wavelength-independent sources located at the canopy bottom ("S problem"). In terms of this approach, the BRDF $\mathbf{r}_k(\Omega_v, \Omega_0, p)$ of a heterogeneous canopy at wavelength λ can be expressed as [7], [8]

$$\mathbf{r}_\lambda(\Omega, \Omega_0) = w_{bs,\lambda} \mathbf{r}_{bs,\lambda}(\Omega_0) + w_{S,\lambda} \mathbf{t}_{S,\lambda} \frac{\rho_{eff}(\lambda)}{1 - \rho_{eff}(\lambda) \cdot \mathbf{r}_{S,\lambda}} \mathbf{t}_{bs,\lambda}(\Omega_0). \quad (2)$$

Here $\mathbf{r}_{bs,\lambda}(\Omega_0)$ and $\mathbf{t}_{bs,\lambda}(\Omega_0)$ are directional hemispherical reflectance (DHR) and canopy transmittance for the black soil

problem, and $\mathbf{r}_{S,\lambda}$ and $\mathbf{t}_{S,\lambda}$ are reflectance and transmittance resulting from an anisotropic source located underneath the canopy. The weight $w_{bs,\lambda}$ is the ratio of the BRDF for the black soil problem to $\mathbf{r}_{bs,\lambda}(\Omega_0)$, and $w_{S,\lambda}$ is the ratio of the canopy leaving radiance generated by anisotropic sources on the canopy bottom to $\mathbf{t}_{S,\lambda}$. The weights $w_{bs,\lambda}$ and $w_{S,\lambda}$ are functions of sun-view geometry, wavelength, and LAI. They are precomputed and stored in the LUT [7].

The effective ground reflectance ρ_{eff} is the fraction of radiation reflected by the canopy ground. It depends on the radiative regime at the canopy bottom. However, its range of variations does not exceed the range of variations of the hemispherically integrated bidirectional factor of the ground surface, which is independent of vegetation [7]. Therefore, ρ_{eff} can be used as a parameter to characterize the ground reflection. The set of various patterns of effective ground reflectances at the MODIS spectral bands is a static table of the algorithm, i.e., the element of the LUT. The present version of the LUT contains 29 patterns of ρ_{eff} ranging from bright to dark. They were taken from the soil reflectance model developed by Jacquemoud *et al.* [25], with model inputs presented in Baret *et al.* [26]. These soil patterns include three soil types: mixtures of clay, sand, and peat. Each soil type is characterized by three moisture levels and three soil roughness types. In biomes with grounds of intermediate brightness, all soil patterns are assigned. In biomes where the ground is bright, the first 16 bright soil patterns are used.

Note that $\mathbf{r}_{bs,\lambda}(\Omega_0)$ and $\mathbf{r}_{S,\lambda}$ are not included in the LUT. Given canopy absorptance ($\mathbf{a}_{bs,\lambda}(\Omega_0)$ and $\mathbf{a}_{S,\lambda}$) and transmittance ($\mathbf{t}_{bs,\lambda}(\Omega_0)$ and $\mathbf{t}_{S,\lambda}$), they are evaluated via the law of energy conservation as

$$\mathbf{r}_{bs,\lambda} + \mathbf{t}_{bs,\lambda} + \mathbf{a}_{bs,\lambda} = 1 \quad (3)$$

$$\mathbf{r}_{S,\lambda} + \mathbf{t}_{S,\lambda} + \mathbf{a}_{S,\lambda} = 1. \quad (4)$$

This makes canopy reflectance sensitive to the within canopy radiation regime $\mathbf{t}_{bs,\lambda}(\Omega_0)$, $\mathbf{a}_{bs,\lambda}(\Omega_0)$, $\mathbf{t}_{S,\lambda}$, $\mathbf{a}_{S,\lambda}$.

The dependence of canopy absorptance on wavelength for the black soil problem (subscript $\kappa = \text{"bs"}$) and S problem ($\kappa = \text{"S"}$) can be derived [7] as

$$\mathbf{a}_{\kappa,\lambda} = \frac{1 - \omega(\lambda_0) p_\kappa}{1 - \omega(\lambda) p_\kappa} \frac{1 - \omega(\lambda)}{1 - \omega(\lambda_0)} \mathbf{a}_{\kappa,\lambda_0}. \quad (5)$$

Here $\omega(\lambda)$ is the leaf albedo (leaf reflectance + leaf transmittance). It is a stable characteristic of green leaves, although its magnitude can vary with leaf age and species. In order to obtain accurate leaf albedos for the six biome types, we obtained leaf spectra data from several sources. Mean leaf reflectance and transmittance values were calculated for the six biome types at seven MODIS bands (645 nm, 859 nm, 469 nm, 555 nm, 1240 nm, 1640 nm, and 2130 nm). We stored the mean albedo in the LUT. Variable p_κ is a wavelength independent coefficient defined as [7], [27]

$$p_\kappa = 1 - \frac{\int_V \int_{4\pi} I_{\kappa,b}(r, \Omega) \sigma(r, \Omega) dr d\Omega}{\int_V \int_{4\pi} I_{\kappa,w}(r, \Omega) \sigma(r, \Omega) dr d\Omega}. \quad (6)$$

Where $I_{\kappa,b}$ and $I_{\kappa,w}$ are solutions of the black soil problem and S problem for black ($\omega = 0$) and white ($\omega = 1$) leaves, and σ is the extinction coefficient (dependent on vegetation types). V is a parallelepiped where vegetation canopies are located. Its height coincides with the height of plants and its horizontal dimension coincides with the size of the pixels. The coefficient p_{κ} depends on canopy structure and V and is an element of the LUT. Because the horizontal dimension of V coincides with the size of pixel, p_{κ} is a resolution dependent parameter. A precise derivation of (5), and (6) is given in [7]. Validation of relationships (6) with field measurements is presented in [27]. Similar relationships are also valid for canopy transmittance [7], [27].

Thus, given canopy absorptance and transmittance for the black soil problem and S problem at a reference wavelength λ_0 , one can evaluate these variables at any other wavelength λ . Therefore, we only store canopy absorptances $\mathbf{a}_{\kappa,\lambda_0}$, transmittances $\mathbf{t}_{\kappa,\lambda_0}$, the coefficients p_{κ} , and leaf albedo, instead of $\mathbf{a}_{\kappa,\lambda}$ and $\mathbf{t}_{\kappa,\lambda}$ in the LUT. Reflectances $\mathbf{r}_{bs,\lambda}(\Omega_0)$ and $\mathbf{r}_{S,\lambda}$ can then be evaluated via the energy conservation law (3) and (4) and inserted into (2).

Similar to (2), the fraction of radiation absorbed by vegetation, $\mathbf{a}_{\lambda}(\Omega_0)$, at wavelength λ can be expressed as [7]

$$\mathbf{a}_{\lambda}(\Omega_0) = \mathbf{a}_{bs,\lambda}(\Omega_0) + \mathbf{a}_{S,\lambda} \frac{\rho_{eff}(\lambda)}{1 - \rho_{eff}(\lambda) \cdot \mathbf{r}_{S,\lambda}} \mathbf{t}_{bs,\lambda}(\Omega_0). \quad (7)$$

For each acceptable solution $p = [\text{canopy, soil}]$, a value of FPAR can be explicitly evaluated as the integral of (7) over the photosynthetically active region of the solar spectrum [7].

C. Physical Meaning of (2)

Any pixel can be depicted as a point in the spectral space. The spectral BRDF's tend to occupy certain well localized space in the spectral space, depending upon the architecture of the biome. We use (2) to explain this behavior in the RED-NIR plane as follows:

- 1) If LAI = 0, then $\mathbf{r}_{bs,\lambda}(\Omega_0) = \mathbf{r}_{S,\lambda} = 0$, $\mathbf{t}_{bs,\lambda}(\Omega_0) = \mathbf{t}_{S,\lambda} = 1$, and $w_{S,\lambda}$ coincides with bidirectional surface reflectance factor [7]. The BRDF at RED and NIR results from photon-ground interactions. The pixels are located on the so-called soil line (around 1:1 line in the RED-NIR spectral space) [26], [28]. The spectral behavior for different soil types will determine the exact location of the soil line. The bright soil pattern will generate high reflectance in RED and NIR. The dark soil pattern will generate low reflectance in RED and NIR.
- 2) A high value of LAI corresponds to a very dense canopy. Its transmittances $\mathbf{t}_{bs,\lambda}(\Omega_0)$ and $\mathbf{t}_{S,\lambda}$ are close to zero and thus, the contribution of soil is minimal. Pixels will occupy a narrow space near the NIR axis. Canopy reflectances at RED and NIR wavelengths characterize exactly the spectral properties of vegetation, that is, plants absorb radiation very efficiently throughout the visible regions and strongly reflect and transmit at NIR. The type of vegetation and its phenology will determine the precise location in the RED-NIR spectral space.

- 3) If LAI is between case 1) and case 2), neither $\mathbf{r}_{bs,\lambda}(\Omega_0)$ nor transmittance will equal zero, and gaps in the vegetation elements will cause photons to interact with soil and canopies. The soil-canopy interactions will cause the canopy response, with a hypothetical nonreflecting soil background, to shift toward the soil line (RED reflectance will decrease, and changes in NIR reflectance will depend on the soil brightness pattern under the canopy) [28]. The location of pixels will be between the soil line and NIR axis. The more gaps, the smaller the LAI value and the closer the pixels are to the soil line.

To summarize, (2) shows how the location of a pixel in the spectral space is related to LAI values. If a pixel is close to the soil line, its LAI value is small. Away from the soil line toward the NIR axis, the contribution of soil to canopy leaving radiance decreases as the product of $\mathbf{t}_{bs,\lambda}(\Omega_0)$ and $\mathbf{t}_{S,\lambda}$, and thus, LAI values increase. The direction of this movement in the spectral space results in different rates of LAI variations. Such a representation of canopy reflectances is used in our algorithm to build and adjust the LUT, and to interpret results presented in Section IV.

D. Adjusting the LUT for Data Resolution

Before the configurable parameters of the LUT can be set, data of a specific spatial resolution must be analyzed to locate the pixels in the spectral space (for example, the RED-NIR space) according to the biome type. We evaluated the data density distribution function as follows: specifying a fine grid cell in the spectral space, counting the number of canopy reflectances in this cell, and then dividing this value by the total number of pixels in the entire spectral space. The data density distribution function was evaluated for each biome type. A location of high density (25% of all pixels) for each biome in the RED-NIR space was plotted and used to adjust the LUT as follows. The areas of 25% density can be interpreted as the sets of pixels representing the most probable patterns of canopy structure. As an example, for biome 5 (broadleaf forests), we located the 25% density of this biome in the spectral space during July, the green season. Then we run the algorithm using only these pixels as input data and plotted the histogram of the retrieved LAI value. Based on previously reported results [24], the most probable canopy realization in this case has an LAI value of about 5. It means that the peak of the histogram should be around five. We adjusted the LUT by changing p_{κ} to represent the corresponding data set so that the simulated BRDF at RED and NIR wavelengths corresponding to LAI = 5 fall in the 25% density plot. Given the location of the most probable realization of canopy structure, (2) can be used to specify the location of pixels at other values of LAI and soil patterns. The LUT was then adjusted for all biomes.

III. DATA ANALYSIS

Before MODIS data are available, data acquired by other instruments can be used to prototype and test the functionality of the LAI-FPAR algorithm. The goal of this section is to describe

and analyze the surface reflectance data used to prototype the algorithm.

A. Satellite Data

LASUR refers to data acquired during 1989-1990 and processed at Centre d'Etudes Spatiales de la Biosphere (CESBIO), Toulouse, France, from AVHRR onboard the NOAA-11 satellite [29], [30]. LASUR is a reprocessing of weekly global vegetation index data [31]. AVHRR is a cross-track scanning system featuring one visible (RED, 572–698 nm), one NIR (716–985 nm), one short wave infrared, and two thermal infrared channels. For LASUR products, data from RED and NIR channels were used to estimate surface reflectances and vegetation index, and data from the two thermal infrared channels were used to estimate the surface temperature. LASUR data were calibrated and corrected for atmospheric effects and filtered to eliminate residual noises and perturbations [29], [30]. The data span is from 75° N to 55° S in latitude, and 180° W to 180° E in longitude. Each image has 904 rows and 2500 columns. The spatial resolution is 1/7th of a degree. In this study, RED and NIR surface reflectances from July 1989, were used to prototype the MODIS LAI/FPAR algorithm. We created a monthly layer based on maximum NDVI compositing of the four weekly layers in this month, minimizing cloud contamination, off-nadir viewing effects, sun-angle effects and aerosol and water vapor effects [32].

A biome classification map (BCM) that describes the global distribution of six canopy structural types (biomes) was used as a prototype of the MODIS land cover product, required by the MODIS LAI/FPAR algorithm. BCM was derived from the AVHRR Pathfinder data set [24] and is time-independent. The six biome types are: grasses and cereal crops (biome 1), shrubs (biome 2), broadleaf crops (biome 3), savannas (biome 4), broadleaf forests (biome 5), and needle forests (biome 6).

We also utilized Landsat Thematic Mapper (TM) scenes of Northwest U.S. (Washington and Oregon) from June 26, 1987 at 30 m resolution to evaluate the algorithm's response to high resolution data. In this study, we used data from band 3 (RED, 630–690 nm) and band 4 (NIR, 760–900 nm). This image was geometrically registered to a terrain-corrected image with an universal transverse Mercator (UTM) projection. The dark object subtraction method of atmospheric correction was used to correct surface reflectance for the atmospheric effect [33], [34]. There was also a "sitemap" containing polygons of known ground cover, associated with this data set. This sitemap distinguished 17 different forest densities, based on the percentage of forest cover in a forested pixel, and seven other types of miscellaneous landcover types. Using the Bayesian maximum likelihood classification method, we separated this image into three biomes, grasses and cereal crops, broadleaf forests and needle forests. We attributed to broadleaf forests all the pixels where hardwood forest makes up more than 60% of the pixel area. Needle forests consist of those pixels in which conifers make up more than 60% of the pixel area. The other landcover classes that do not belong to these three biomes were defined as unknown class types. In total, grasses occupy 6.6% of the total area, and broadleaf and needle forests occupy 4.8% and 10.3% of the total area.

B. Spectral Signatures

Although all the vegetation types have relatively similar spectral properties (large absorption in RED and large reflectance in NIR), different biomes have special characteristics depending on the canopy architecture. These characteristics can be distinguished by comparing the spectral signatures. Fig. 1(a) and (b) present histograms of canopy reflectances in RED and NIR spectral bands as a function of biome type derived from LASUR data. In the RED band, canopy reflectances vary between 0.0 and 0.2. Broadleaf and needle forests have the strongest absorption features. On average, they reflect only 3% and 4.5% (Table I) of the incoming radiation. Grasses and broadleaf crops are characterized as the brightest biomes. About 8% and 6.5% of the incoming radiation is reflected. In the NIR band, reflectances vary between 0.1 and 0.5. Shrubs and broadleaf crops represent two extremes. Their reflectances, on average, are 21% and 32%, respectively. The other biomes reflect nearly 25% of the incoming radiation and have similar histograms.

Vegetation indices typically capture the absorption contrast across the 650-850 nm wavelength interval through combinations of broadband RED and NIR reflectance. The most widely used index in the processing of satellite data is NDVI, defined as $(\rho_N - \rho_R)/(\rho_N + \rho_R)$, where ρ_N and ρ_R are spectral reflectance at NIR and RED wavelengths, respectively. It is a measure of chlorophyll abundance and energy absorption [35]. Fig. 1(c) demonstrates the distribution of NDVI values derived from LASUR data. In general, broadleaf forests have the highest NDVI values, around 0.813, followed by needle forest, around 0.695 (Table I). Broadleaf crops and savannas have similar NDVI distributions, and their NDVI values are larger than those of grasses (0.515) and shrubs (0.615). It would be difficult to distinguish broadleaf crops from savannas using only NDVI.

The data density distribution function, introduced earlier in Section II, can be used to indicate the location of a data peak in the spectral space. Fig. 1(d) shows the location of points with high density for different biomes in the RED-NIR space. Each area bounded by the contour represents an area containing the 25% density of the total pixels from a given biome type. Each biome tends to cluster and occupy a well localized space. Broadleaf forests are located at low RED and high NIR area, while grasses are at the high RED and low NIR area. Broadleaf crops and savannas occupy different locations, although their NDVI distributions are comparable. In general, the more unique a location, the better the ability to distinguish each of the vegetation type. The influence of soil is also clear from this panel. Grasses and shrubs are biomes located near the soil line. Broadleaf forests are dense vegetation and located closest to the NIR axis.

Fig. 2 presents canopy reflectance features from Landsat data. On average, grasses, broadleaf and needle forests reflect only 6.5%, 2%, and 1.3%, respectively, of the incoming radiation in the RED band (Table I). This is much less than that of LASUR data. However, the NIR reflectance of grasses and broadleaf forest can be as high as 30% and 34.8%, compared with 25% and 29% for the LASUR data. Needle forests are the darkest

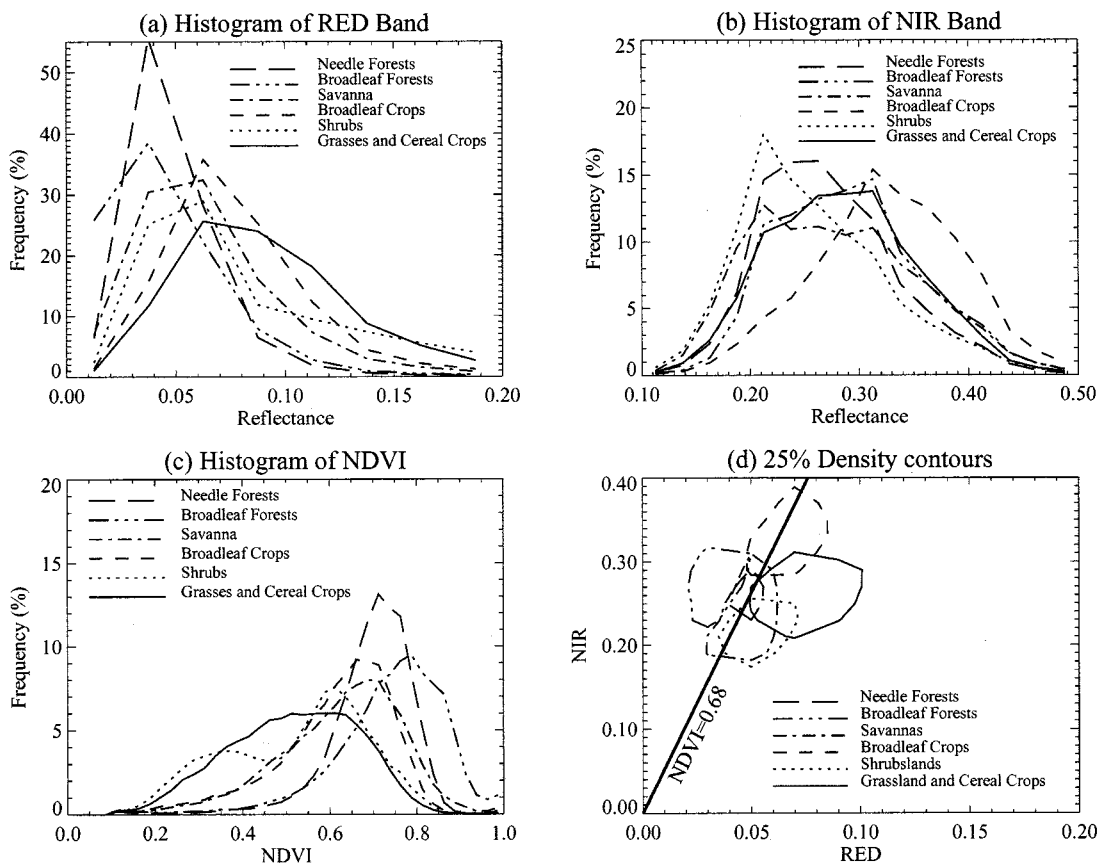


Fig. 1. Statistical properties of canopy reflectances for global LASUR data in July 1989. (a) Histogram of canopy reflectances at the RED band. (b) Histogram of canopy reflectances at the NIR band. (c) Histogram of NDVI. (d) 25% density contours in the RED-NIR space, which shows the location of points with high density for different biomes. The straight line represents the place where NDVI are equal to 0.68. Canopy structure varies considerably with the same NDVI value.

TABLE I
SPECTRAL STATISTICS FOR LASUR DATA AND LANDSAT TM DATA

LASUR DATA			
Biome Type	Mean Red	Mean NIR	Mean NDVI
Grasses and Cereal Crops	0.080	0.25	0.515
Shrubs	0.050	0.21	0.615
Broadleaf Crops	0.065	0.32	0.662
Savanna	0.050	0.23	0.645
Broadleaf Forests	0.030	0.29	0.813
Needle Forests	0.045	0.25	0.695
LANDSAT DATA			
Biome Type	Mean Red	Mean NIR	Mean NDVI
Grasses and Cereal Crops	0.065	0.304	0.635
Broadleaf Forests	0.022	0.348	0.881
Needle Forests	0.013	0.200	0.886

among the three biomes, both at RED and NIR. The NDVI values for the three biomes are 0.635, 0.881, 0.886, respectively (Table I). The 25% density contours are tightly clustered occupying a small but unique location in the spectral space. At the same time, the clusters are away from the soil line, and closer to the NIR axis. The biomes are well separated that they do not overlap even on the 75% density contour.

Comparing the results from the previous two data sets, we conclude that, as the spatial resolution increases from LASUR

data to Landsat data, the reflectance decreases in the RED band and increases in the NIR band, and consequently, fewer biomes overlap in the RED-NIR spectral space.

IV. PROTOTYPING OF THE ALGORITHM

A. Prototyping with LASUR Data

This section describes global LAI and FPAR fields derived with the MODIS LAI/FPAR algorithm using the LASUR data.

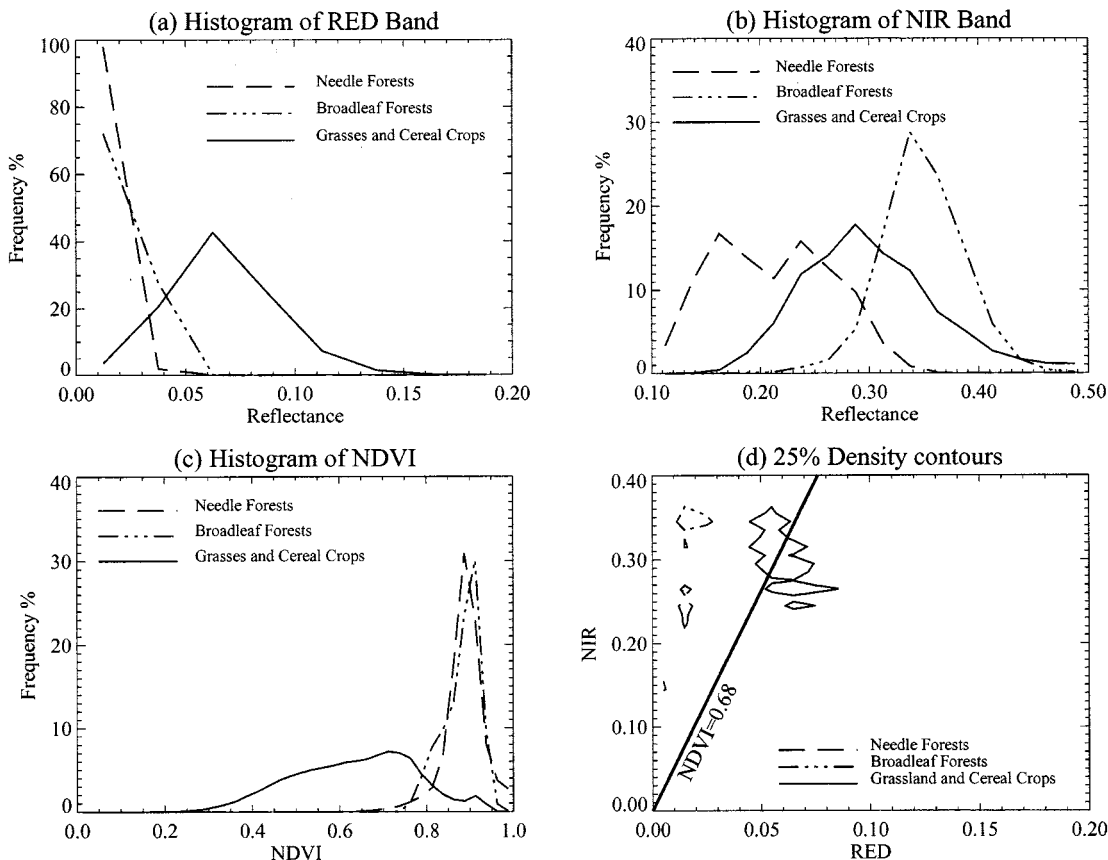


Fig. 2. Statistical properties of canopy reflectances for Landsat TM data of northwest U.S. in June 1987. (a) Histogram of canopy reflectances at the RED band. (b) Histogram of canopy reflectances at the NIR band. (c) Histogram of NDVI. (d) 25% density contours in the RED-NIR space, which shows the location of points with high density for different biomes. The straight line represents the place where NDVI are equal to 0.68.

The objectives are to analyze these fields and situations when the algorithm fails to retrieve a value of LAI/FPAR, and to assess the influence of uncertainties in surface reflectances on the LAI/FPAR product quality.

The algorithm was run pixel-by-pixel using LASUR data and land cover BCM on all pixels with NDVI greater than 0.1. The following notions are used in discussion on algorithm performance. First, a pixel for which the algorithm retrieves a value of LAI is a “retrieved” pixel. Second, a pixel for which the algorithm can not retrieve a value of LAI is termed a “nonretrieved” pixel, and the algorithm is said to have failed for this pixel. Third, the ratio of the number of retrieved pixels to the total number of pixels is the retrieval index (RI).

1) *Input Data*: Atmospherically-corrected surface reflectances and uncertainties in measurements and simulations are inputs to the algorithm (1). However, LASUR reports no information on reflectance uncertainties. Therefore, the uncertainties were simulated as

$$\delta_{RED} = \delta_{NIR} = \varepsilon [d_{RED}^2 + d_{NIR}^2]^{1/2}. \quad (8)$$

Here, ε is the mean uncertainty and is assumed to be a constant in this study. Fig. 3 demonstrates the dependence of the RI on ε . The RI increases with increases in ε . However, the quality of retrieved LAI/FPAR decreases with increases in ε . If ε is underestimated, the algorithm fails even though surface reflectances

were reasonable. If ε is overestimated, the algorithm can produce LAI/FPAR values for nonvegetated pixels. Finding ε for which about 95% of nonretrieved pixels are nonvegetated is a solution to the above problem, which was 0.2 for the LASUR data. The RI varies with biome types at a constant ε . When ε is 0.2, the RI for the six biomes is 91.5%, 92.7%, 74.0%, 79.7%, 39.3%, 54.5%, respectively. The reason that broadleaf and needle forests have low RI could be due to dark soil patterns used to represent effective ground reflectance ρ_{eff} in (2). If a pixel is bright, it will not be considered as a pure broadleaf or needle forest pixel and, consequently, the algorithm will fail. Low values of RI are not necessarily an indication of poor performance of the algorithm. For the coarse resolution data, such as LASUR (1/7th of a degree), the vegetation in the pixel may be a case of mixture of different land cover classes. Therefore, biome-specific spectral features may be lost. At the present time, restricting the algorithm to pure vegetation types retains the ability to discriminate biome types.

2) *Histograms of LAI and FPAR*: The histogram of the retrieved LAI/FPAR describes the value distribution of these fields for various biomes. Fig. 4(a) presents the histogram of retrieved LAI using the LASUR data. Broadleaf and needle forests have distributions distinct from the other four biomes. The former have relatively high LAI values, concentrated about 4.0 to 6.0. For the latter, the LAI values are generally less than 2.0. The differences among grasses, shrubs, broadleaf crops, and savannas

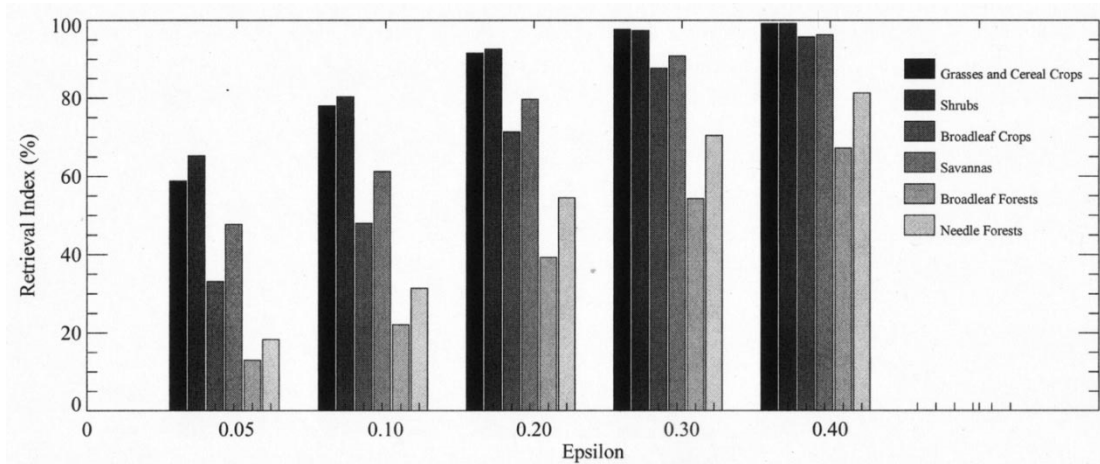


Fig. 3. Dependence of the retrieval index (RI) on uncertainties ϵ in measurements and simulations.

are seen in the peak and tail of the LAI histograms. The highest frequency of LAI for broadleaf crops and savannas is around 1.25, for grasses around 1.0, and for shrubs around 0.75 and 1.25. The distribution tail of broadleaf crops and savannas contains at least 20% of the pixels whose LAI values are larger than 4.0. The tail ends at about 4.0 for grasses and shrubs. Therefore, the mean LAI for broadleaf crops and savannas are 2.1 and 2.2, for grasses and shrubs, only 1.2 and 1.4. Shrubs have two obvious peaks that correspond to the two peaks in the NDVI histogram shown in Fig. 1(c). However, the retrieved LAI is not based on the NDVI.

The LAI distribution from a NDVI-based algorithm developed earlier by Myneni *et al.* [24] is shown in Fig. 4(b). The data used for this NDVI-based algorithm were AVHRR Pathfinder data from July 1981 through June 1991. The average July retrievals over the ten-year period are shown in this figure. There are many similarities between Fig. 4(a) and (b). Broadleaf and needle forests have much higher LAI than the other four biomes. The double peak in shrubs is also seen in Fig. 4(b). The similarity between the two retrievals imbues confidence in the MODIS algorithm.

Fig. 4(e) and (f) show the NDVI histograms from retrieved and nonretrieved pixels. Compared to Fig. 1(c), the NDVI histogram of retrieved pixels is similar to the NDVI histogram of all pixels. Therefore, the algorithm identifies most of the features in the observed data. Failures are typically two cases. First, NDVI is too high for a particular biome. For example, the algorithm fails to retrieve information when the NDVI of grasses is larger than 0.75. In the LUT, there is no information for grasses at such values of NDVI. Second, for the same NDVI value, some of the pixels are retrieved pixels, but the others are not. The failure of this type will be discussed later.

3) *Test of Physics*: There are many examples in published literature about the strong relation between NDVI and LAI and FPAR [9]–[15]. This provides an opportunity to test the physics of the algorithm by comparing the LAI-NDVI and FPAR-NDVI relationships derived from the algorithm with those reported from field measurements. Fig. 5(a) and (b) shows the distributions of the retrieved values of LAI and FPAR with respect to the NDVI of biome 5. LAI is nonlinearly proportional

to NDVI, while FPAR is linearly proportional to NDVI. This corresponds to relations reported in the literature [24], [36]. Note the NDVI in this plot is evaluated from measured RED and NIR reflectances, while the retrieved quantities result from the algorithm that uses reflectances instead of NDVI. The advantages of using the MODIS algorithm instead of NDVI relations are as follows. First, NDVI-LAI relations are subject to changes in sun angle, background reflectance, and view angle, while the MODIS algorithm actually uses these changes as sources of information in the retrieval process. Second, NDVI is based on two spectral bands only, while the algorithm can ingest 3, 4, or even MODIS 7 bands simultaneously to retrieve LAI and FPAR.

Fig. 5(c) and (d) shows the scatter plot of data from retrieved and nonretrieved pixels in the RED-NIR plane. This distribution provides insights into where and why the algorithm failed. For retrieved pixels in the RED-NIR plane, canopy reflectances range about 0.02–0.16 for the RED band and 0.1–0.42 for the NIR band. This reflectance space obviously overlaps the 25% density contour area. From Figs. 4(e), (f) and 5(c), (d), it appears that there are three regions where the algorithm fails. RED reflectance less than 0.03 (NDVI is very large), large RED and NIR reflectances (pixels are near the soil line and NDVI is very small), and RED and NIR are relatively large and located between the first two regions. When the RED reflectance is very small, the uncertainty is large, and the probability of retrieval decreases. When a pixel is near the soil line, it is not a vegetated pixel, and the algorithm identifies it correctly. For the third region, consider a line, on which NDVI is constant [Fig. 5(d)], in the RED-NIR spectral space. For the same value of NDVI, some pixels result in retrievals, while others do not. The algorithm is sensitive to canopy reflectances on a constant NDVI line, while the NDVI-based algorithm is insensitive to these. It is clear that the algorithm uses information on the canopy spectral properties instead of NDVI, especially, when there are many spectral bands and multi-angle data. Only when a pixel falls within the specified spectral and angular space in the LUT can it retrieve an LAI value. Otherwise, the algorithm fails even if the NDVI is reasonable. Therefore, a correct LUT is a key factor in algorithm performance.

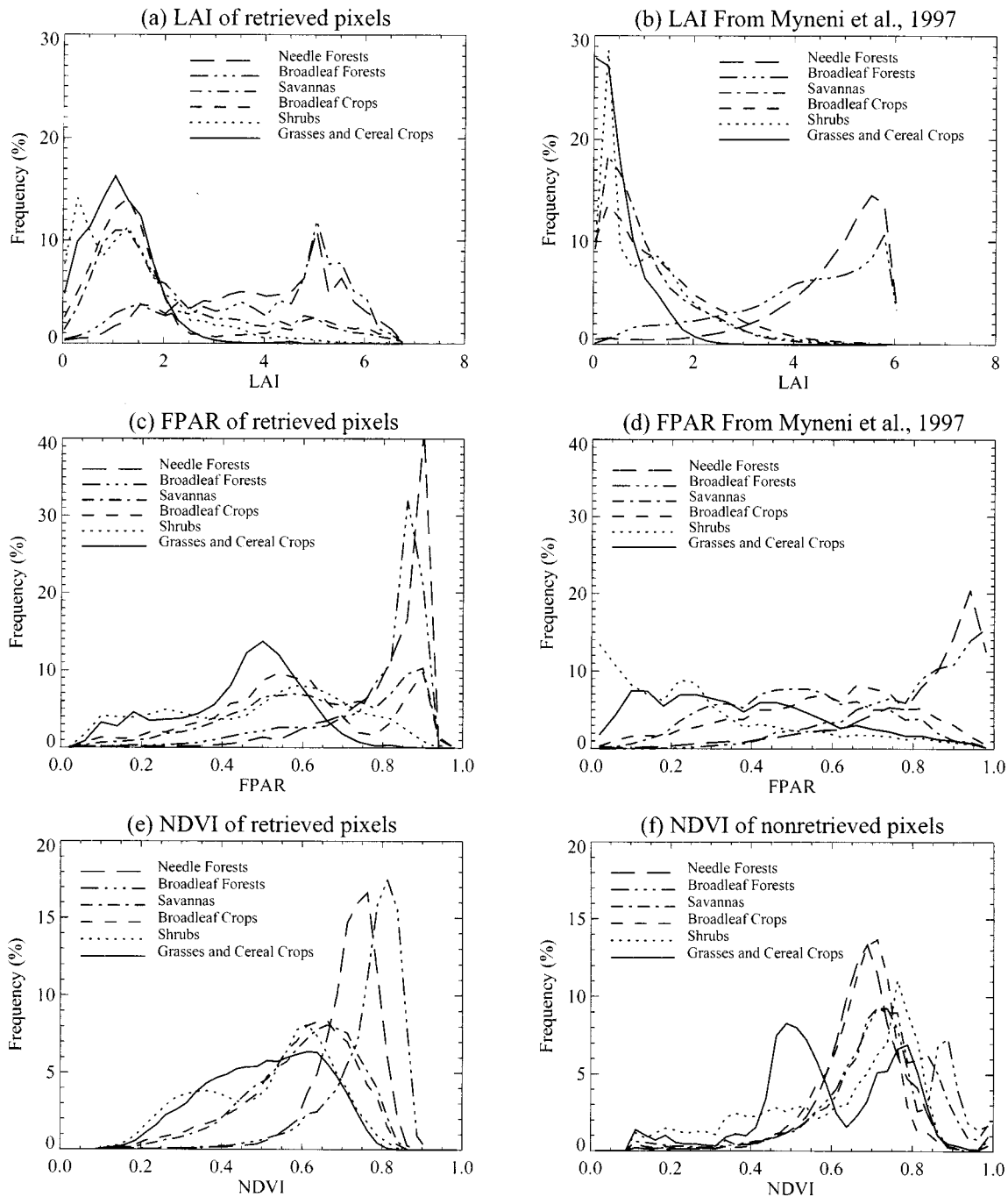


Fig. 4. (a), (c) Histograms of LAI/FPAR derived from the MODIS algorithm with LASUR data. (b), (d) Histograms of LAI/FPAR derived from NDVI-based algorithm with ten-year averaged AVHRR Pathfinder data [24]. (e) Histogram of NDVI from retrieved pixels. (f) Histogram of NDVI from nonretrieved pixels. The mean uncertainty ε is 0.20.

4) *Reliability of Retrieved LAI/FPAR*: Equation (1) may admit a number of solutions, covering a wide range of LAI values. When this happens, the canopy reflectances are said to belong to the saturation domain, being insensitive to various parameter values characterizing the canopy. The algorithm can recognize this situation. The frequency with which LAI values are retrieved under the condition of saturation is termed saturation frequency. The accuracy of retrievals decreases in the case of saturation, that is, the information conveyed about canopy structure by canopy reflectances is small because a wide range

of natural variations in canopy structure and soil can result in the same value of remotely-sensed signal [8]. Therefore, the saturation frequency and threshold LAI value of saturation are important criteria when assessing the accuracy of retrievals. For the six biomes, the overall saturation frequencies are 0.38%, 2.5%, 16%, 15%, 48.5%, and 42.5%, respectively. Fig. 6(a) shows the histogram of LAI retrieved under the condition of saturation for the six biomes. When the LAI is less than 4.0, the saturation frequency is low for all biomes. But, when LAI is larger than 4.0, the saturation frequency drastically increases.

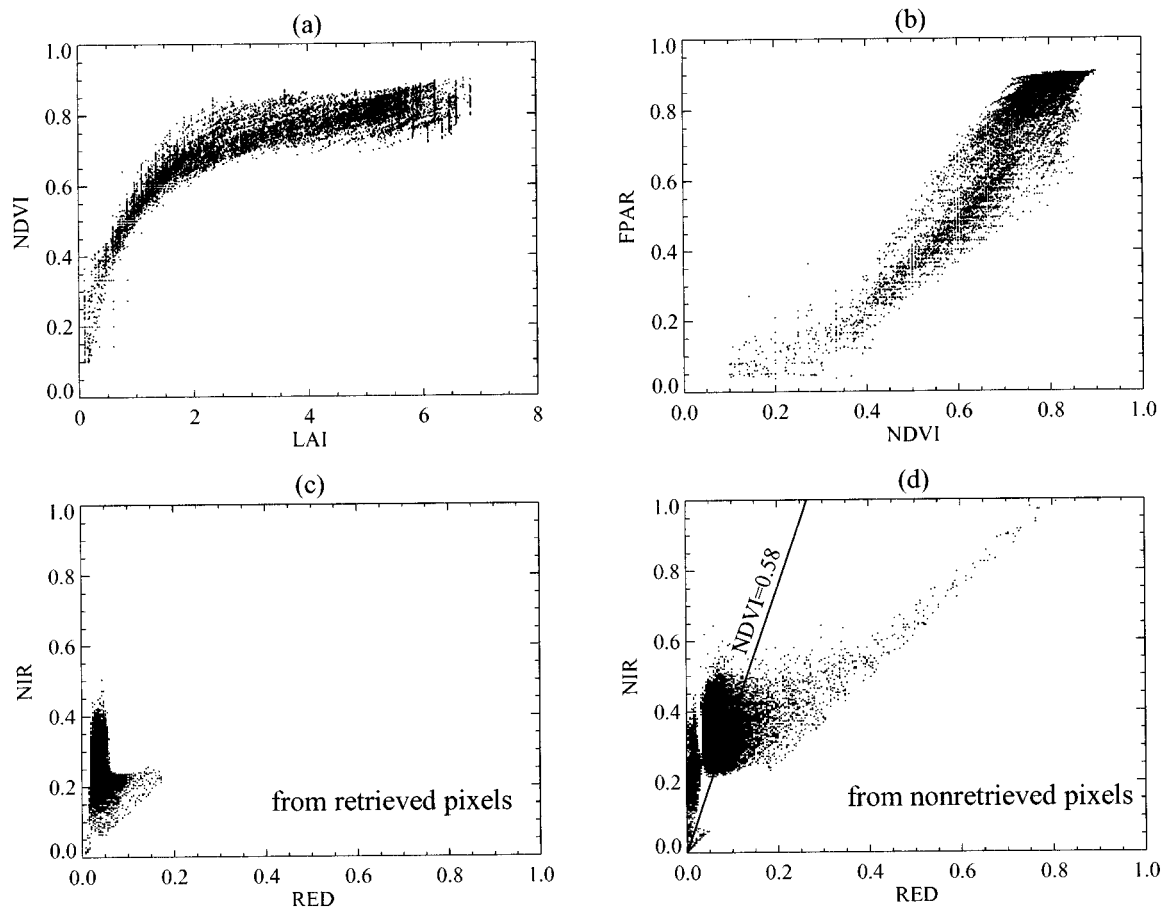


Fig. 5. For broadleaf forests in LASUR data, the scatter plot shows (a) the LAI-NDVI relationship, (b) the NDVI-FPAR relationship, (c) retrieved pixels in the RED-NIR space, and (d) nonretrieved pixels in the RED-NIR space.

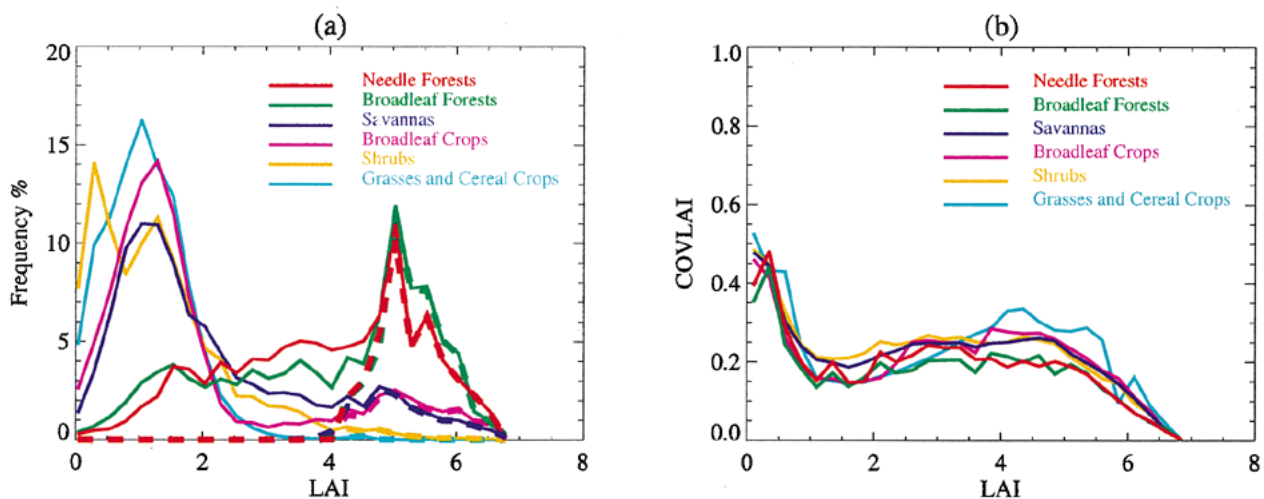


Fig. 6. (a) Histogram of LAI values retrieved under the condition of saturation. Solid lines present the same histograms as Fig. 4(a). Dashed lines show the ratio of the number of LAI values retrieved under the condition of saturation to the total number of retrieved pixels. (b) Coefficient of variation (standard deviation/mean) of retrieved LAI values (COVLAI) as a function of retrieved LAI.

Nearly every pixel is retrieved under the condition of saturation when the LAI is larger than 5.0.

Broadleaf and needle forests in general have high LAI values, and therefore, a high saturation frequency. In order to assess the quality of retrieved LAI/FPAR values, we examine the coefficient of variation of the retrieved LAI value (COVLAI) defined

as the ratio of LAI dispersion to mean LAI evaluated from the set of acceptable solutions. The lower the COVLAI value, the more reliable and accurate the retrieval. Fig. 6(b) demonstrates COVLAI as a function of retrieved LAI and biome types. The COVLAI values vary around 0.2, while the standard deviations of the retrievals increase with LAI. This is not surprising, be-

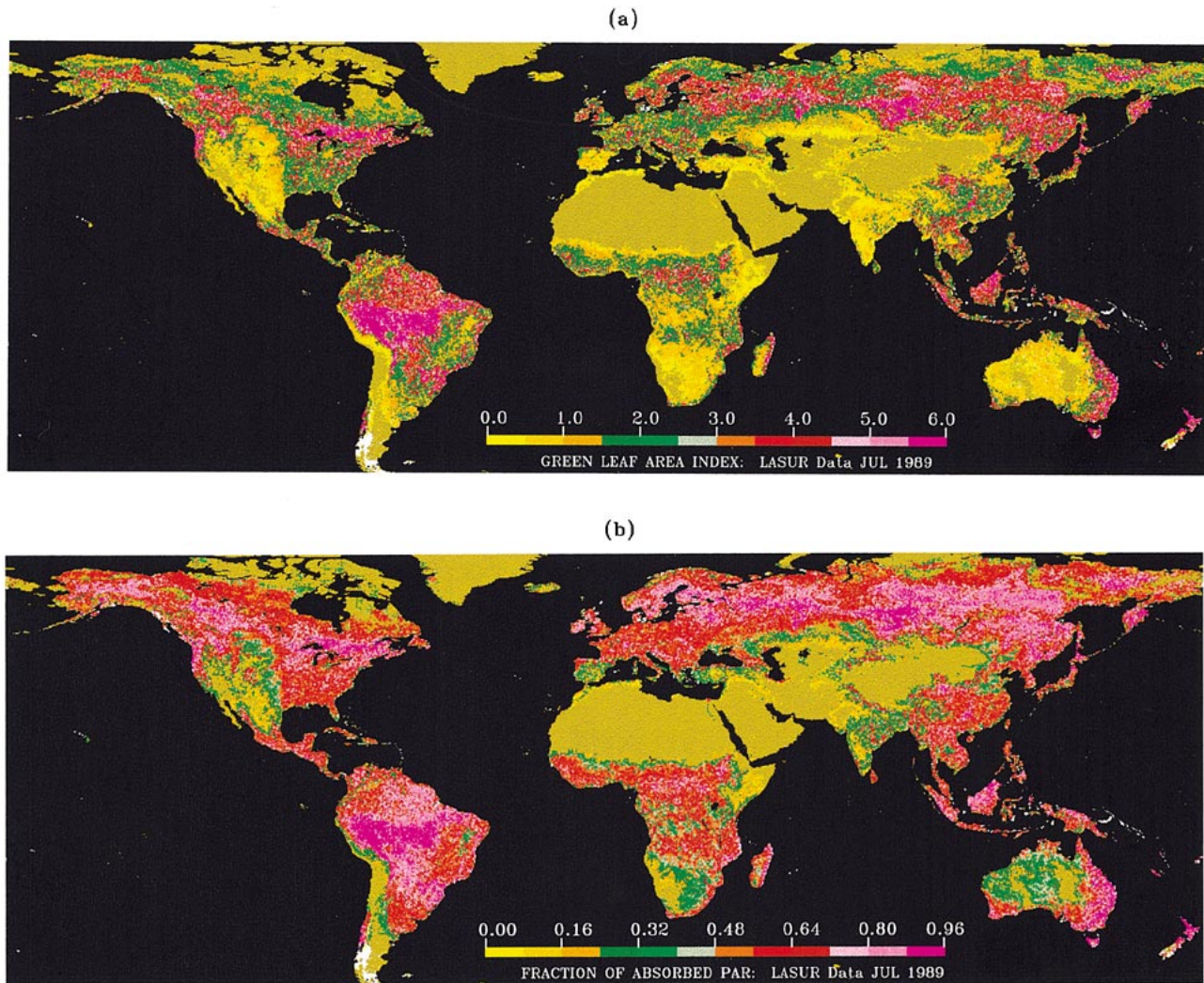


Fig. 7. (a) Global LAI and (b) global FPAR fields derived from LASUR data in July, 1989. For the nonretrieved pixels, the LAI-NDVI, and NDVI-FPAR relations were used to estimate LAI and FPAR.

cause at high LAI values the reflectances belong to the saturation domain and it is difficult to localize a single estimate. When LAI is larger than 3.0, broadleaf and needle forests have relatively lower COVLAI values than other biomes at the same LAI value. Therefore, when LAI is large and saturation frequency is large, the retrieval is not necessarily poor. COVLAI cannot be less than 0.2, because the mean uncertainty in these runs is 0.2. The quality of the retrievals cannot be better than the quality of the largest uncertainty in spectral reflectance data input to the algorithm. Therefore, the availability of band specific uncertainties in atmospherically corrected surface reflectances is critical to assess the quality of the LAI/FPAR product.

5) *LAI and FPAR Images*: The algorithm was run on the global LASUR data for the month of July 1989. For the nonretrieved pixels, the averaged NDVI-LAI/NDVI-FPAR relations derived from all the retrieved pixels were used to estimate LAI and FPAR. Fig. 7 shows color-coded images of global LAI and FPAR. These compare well with the fields reported earlier by Myneni *et al.* [24]. The comparison was done to assess if the algorithm captures the general patterns of LAI and FPAR dis-

tribution at the global scale. Whether the retrievals are accurate or not requires validation, which is the next step.

6) *Biome Misclassification and LAI/FPAR Retrievals*: The MODIS LAI/FPAR algorithm requires a land cover classification map provided by the MODIS land cover product [22]. It is important, therefore, to assess the impact of biome misclassification on LAI/FPAR retrievals. We ran the algorithm six times per pixel, each time using a different biome's LUT. This simulates the effects of biome misclassification on LAI/FPAR retrievals. The results are shown in Table II. Typically, when pixels are misclassified, either the RI is low and/or the retrieved LAI values are incorrect. When misclassification between distinct biomes occurs, the results are predictable. For example, grasses and cereal crops (biome 1) and broadleaf forests (biome 5) are distinct in their architecture and foliage optics. If biome 1 is misclassified as biome 5, the RI is 27% compared to 91% without misclassification. Or, if biome 5 is misclassified as biome 1, the retrieved LAI value decreases from 4 or 5 to 2. Misclassification can be detected by the RI, mean LAI and the histogram of retrieved LAI distribution in such cases. If misclas-

TABLE II
(a) SUCCESS INDEX AND (b) MEAN LAI FOR MISCLASSIFIED LASUR DATA

		Misclassified Biome Type					
		Grasses And Cereal Crops	Shrubs	Broadleaf Crops	Savanna	Broadleaf Forests	Needle Forests
BCM Biome Type	Grasses and Cereal Crops	91.53	88.54	89.60	88.68	27.63	29.00
	Shrubs	87.67	92.66	91.53	91.73	47.34	46.37
	Broadleaf Crops	87.93	70.33	74.03	71.29	14.80	19.52
	Savanna	78.02	79.91	80.25	79.65	41.31	44.33
	Broadleaf Forests	55.02	63.23	61.4	61.32	39.30	33.59
	Needle Forests	76.75	85.74	84.92	84.78	46.38	54.54

(a)

		Misclassified Biome Type					
		Grasses And Cereal Crops	Shrubs	Broadleaf Crops	Savanna	Broadleaf Forests	Needle Forests
BCM Biome Type	Grasses and Cereal Crops	1.197	1.245	1.401	1.363	1.293	2.011
	Shrubs	1.026	1.408	1.542	1.514	1.505	1.987
	Broadleaf Crops	1.845	1.833	2.097	2.044	2.424	3.710
	Savanna	1.508	2.079	2.286	2.250	2.221	2.953
	Broadleaf Forests	1.921	3.299	3.439	3.451	4.014	4.649
	Needle Forests	1.640	2.916	3.205	3.179	2.976	3.996

(b)

sification happens between spectrally and structurally similar biomes, perhaps, because of coarse spatial resolution, the impact on LAI/FPAR retrievals is difficult to assess. As an example, consider shrubs (biome 2) and savannas (biome 4). The RI and mean LAI do not vary greatly. The retrieved LAI/FPAR values are acceptable, although the pixels have been misclassified. This example indicates that various biome LUT's share similar entries for certain combinations of spectral reflectances.

B. Prototyping with Landsat Data

1) *General Results:* The MODIS LAI/FPAR algorithm was prototyped with Landsat data for three biomes: grasses and cereal crops, broadleaf forests, needle forests. A fine resolution LUT was used to retrieve LAI and FPAR because of the finer spatial resolution of Landsat data. The RI's for the three vegetation types are 90.7%, 53.9%, 57.9%, respectively, and the mean LAI values are 1.87, 5.79, 4.11, respectively. Compared to

LASUR data, the RI increase for broadleaf and needle forests, and so do the mean LAI values. The saturation frequencies at high LAI values for these biomes are comparable to those reported earlier for LASUR data.

The following explains the dependency of the LUT on spatial resolution. Canopy spectral properties are a function of spatial resolution (Figs. 1 and 2). In the RED-NIR plane of 25% density contours, fine resolution data tend to cluster and occupy a small region close to the NIR axis. Contours corresponding to different biome types do not overlap either. As the resolution decreases, the spectral properties of each biome are influenced by the presence of soil and water as well as the other vegetation types. In the spectral space, the distance between the biomes decreases and the biomes become similar. Therefore, the LUT should reflect these changes in vegetation canopy spectral properties with changes in resolution. The parameters p_{κ} , $\kappa = "bs"$ or "S," introduced by (6) control the dependency of

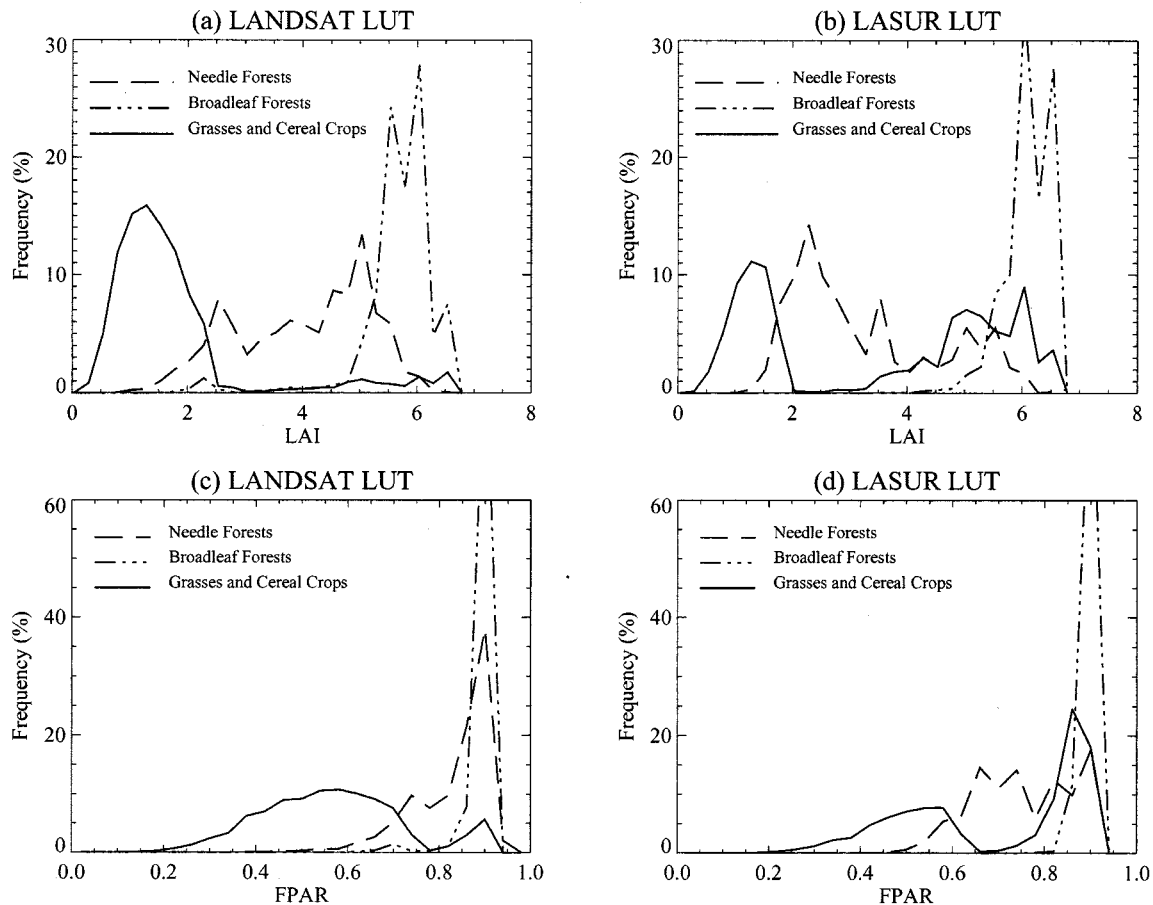


Fig. 8. Retrievals from Landsat data as a function of spatial resolution-dependent look-up table (LUT). Histograms of LAI from (a) Landsat LUT, (b) LASUR LUT, (c) histograms of FPAR from Landsat LUT, and (d) LASUR LUT.

LUT on the spatial resolution of data. To further investigate, the algorithm was performed on Landsat data with LASUR LUT, that is, fine resolution data with coarse resolution LUT. Fig. 8 shows the histogram of LAI and FPAR obtained from Landsat data with LASUR LUT and, also, Landsat data with Landsat LUT. When Landsat data and Landsat LUT are used, the retrieved LAI values vary from 0.0 to 2.5 for grasses, from 5.0 to 7.0 for broadleaf forest, and from 1.5 to 6.0 for needle forests (Table III). When LASUR LUT is used with Landsat data, the histograms of retrieved LAI and FPAR change greatly. For example, the LAI of grasses/cereal crops can reach unrealistic values between 4.0 and 6.0. The LAI of needle forests is concentrated between 1.5 to 4.0, a relatively small range for this biome. The RI for the three biomes also decrease to 87.5%, 39.2%, 4.7%, respectively. When the algorithm is run using LASUR data but with Landsat LUT (Fig. 9), the mean LAI for all biomes decrease, and the differences between forests (high LAI) and other biomes (low LAI) disappear. FPAR shows similar changes. This clearly indicates the dependency between data resolution and the LUT.

2) *Soil or Background Effects:* As previously mentioned, in the design of the MODIS LAI/FPAR algorithm, the 3-D radiative transfer problem can be represented as the sum of two components. The first describes the radiation regime within the vegetation canopy with a completely absorbing soil or background beneath the canopy. The second component describes

additional radiation due to interactions between the soil and vegetation. Therefore, the soil-vegetation interaction is an important component controlling the spectral behavior of vegetation canopies. At the fine resolution, the contribution of the soil-vegetation interaction is negligible in the case of dense vegetation, such as forests. We executed the algorithm only with the black soil problem on Landsat data to test this assumption. The RI can be as high as 50.6% (broadleaf forest) and 54.3% (needle forest), compared to 53.7% and 57.9% if the contribution from the soil-vegetation interaction is added. The histograms of retrieved LAI and FPAR do not change substantially. Therefore, the fine resolution Landsat data represent pure and dense vegetation with minimal soil or background effects in this instance. The RI are only 31% and 45% for broadleaf and needle forests when only the black soil problem is used to retrieve LAI and FPAR for the coarser resolution LASUR data. The soil-vegetation interaction is an important component that controls the spectral behavior of vegetation canopies. Its effect becomes large as the resolution decreases.

V. CONCLUSIONS

Results from the prototyping described in this paper demonstrate the ability of the algorithm to produce global LAI and FPAR fields. For global LASUR data in July, the mean LAI of broadleaf and needle forest is around 4.0, broadleaf crops and

TABLE III
COMPARISON OF THE RESULTS FROM LASUR LUT AND LANDSAT LUT RETRIEVALS

Biome Type	LASUR DATA			
	LASUR LUT		LANDSAT LUT	
	Retrieval Index	Mean LAI	Retrieval Index	Mean LAI
Grasses and Cereal Crops	91.53	1.20	91.6	1.07
Shrubs	92.66	1.41	96.4	0.92
Broadleaf Crops	74.03	2.09	80.1	1.17
Savanna	79.65	2.25	85.4	1.61
Broadleaf Forests	39.30	4.01	41.8	2.62
Needle Forests	54.54	3.99	41.8	1.66

Biome Type	LANDSAT DATA			
	LANDSAT LUT		LASUR LUT	
	Retrieval Index	Mean LAI	Retrieval Index	Mean LAI
Grasses and Cereal Crops	90.7	1.87	87.5	3.62
Broadleaf Forests	53.9	5.79	39.2	6.21
Needle Forests	57.9	4.11	4.7	3.39

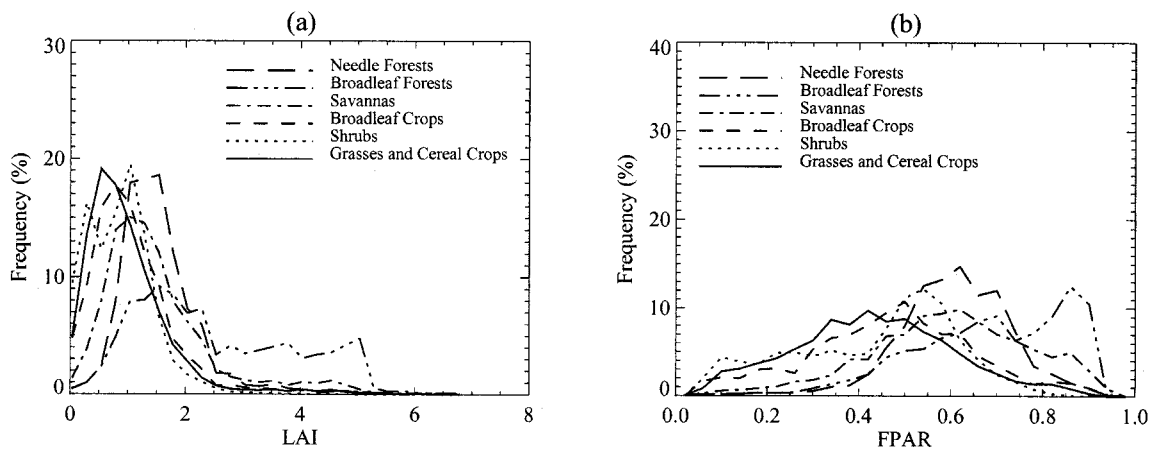


Fig. 9. Retrievals from LASUR data using Landsat look-up table (LUT). Histograms of (a) LAI and (b) FPAR.

savannas 2.1 and 2.2, shrubs 1.4 and grasses and cereal crops 1.2. The algorithm utilizes leaf spectral properties and canopy structural attributes, instead of NDVI, in the retrieval process. An LAI value can only be retrieved when a pixel falls within the specified spectral and angular space in the LUT. The algorithm fails even if the NDVI value is reasonable. The uncertainties in input data influence the RI. RI increases with increasing uncertainties. However, the quality of retrieved LAI/FPAR decreases with increasing uncertainties. A value of 0.2 was found optimal in this study. Quantitatively, the saturation frequency and coefficient of variation (standard deviation/mean) of retrieved LAI values (COVLAI) are two useful metrics to assess the quality of the retrieved field. The higher the saturation frequency and COVLAI value, the lower the quality of the retrieval. On average, if LAI is larger than 4.0, saturation problems begin to influence the retrieval. Forests have higher saturation frequencies than other vegetation types. However, they have lower COVLAI values than other biomes at the same LAI value, especially at high LAI values. Therefore, the retrieval quality is not necessarily poor. COVLAI cannot be less than the total uncertainty in

the data and the LUT, because the quality of the retrievals cannot be better than the quality of the largest uncertainty in spectral reflectance data input to the algorithm. The effect of biome misclassification between distinct biomes on the algorithm can be evaluated through the RI, mean LAI, and the histogram of the retrieved LAI distribution. Misclassification can fatally impact the quality of the retrieval in this case. The impact of biome misclassification between spectrally and structurally similar biomes is negligible, particularly if the spatial resolution of the input data is coarse.

Leaf canopy spectral properties differ with spatial resolution. Each vegetation type in Landsat data tends to cluster and occupy a small region close to the NIR axis in the spectral space, while biomes become spectrally similar in the case of coarse resolution LASUR data. The algorithm is dependent on the spatial resolution of the data through the use of the LUT. We cannot use Landsat LUT to retrieve LASUR LAI/FPAR and vice versa. By evaluating the data density distribution function, we can adjust the algorithm for data resolution and utilize the algorithm with data from other sensors.

ACKNOWLEDGMENT

The authors would like to thank Dr. M. Pax-Lenney and Dr. C. E. Woodcock for the Landsat TM data, as well as two anonymous reviewers for their careful critiques, which greatly improved the quality and readability of the manuscript.

REFERENCES

- [1] P. J. Sellers and D. S. Schmid, "Remote sensing of the land biosphere and biogeochemistry in the EOS era: Science priorities, methods and implementation—EOS land biosphere and biogeochemical cycles panels," *Global Planetary Change*, vol. 7, pp. 279–297, 1993.
- [2] C. S. Potter, J. T. Randerson, C. B. Field, P. A. Matson, P. M. Vitousek, H. A. Mooney, and S. A. Klooster, "Terrestrial ecosystem production: A process model based on global satellite and surface data," *Global Biogeochem. Cycles*, vol. 7, pp. 811–841, 1993.
- [3] S. D. Prince, "A model of regional primary production for use with coarse resolution satellite data," *Int. J. Remote Sens.*, vol. 12, pp. 1313–1330, 1991.
- [4] P. J. Sellers, R. E. Dickinson, D. A. Randall, A. K. Betts, F. G. Hall, J. A. Berry, G. J. Collatz, A. S. Denning, H. A. Mooney, C. A. Nobre, N. Sato, C. B. Field, and A. Henderson-Sellers, "Modeling the exchange of energy, water, and carbon between continents and atmosphere," *Science*, vol. 275, pp. 602–609, 1997.
- [5] S. W. Running and J. C. Coughlan, "A general model of forest ecosystem processes for regional applications. I. Hydrologic balance, canopy gas exchange and primary production processes," *Ecol. Model.*, vol. 42, pp. 125–154, 1988.
- [6] S. W. Running and S. T. Gower, "FOREST-BGC, a general model of forest ecosystem processes for regional applications, II. Dynamic carbon allocation and nitrogen budgets," *Tree Phys.*, vol. 9, pp. 147–160, 1991.
- [7] Y. Knyazikhin, J. V. Martonchik, R. B. Myneni, D. J. Diner, and S. Running, "Synergistic algorithm for estimating vegetation canopy leaf area index and fraction of absorbed photosynthetically active radiation from MODIS and MISR data," *J. Geophys. Res.*, vol. 103, pp. 32 257–32 275, 1998.
- [8] Y. Knyazikhin, J. V. Martonchik, D. J. Diner, R. B. Myneni, M. M. Verstraete, B. Pinty, and N. Gobron, "Estimation of vegetation canopy leaf area index and fraction of absorbed photosynthetically active radiation from atmosphere-corrected MISR data," *J. Geophys. Res.*, vol. 103, pp. 32 239–32 256, 1998.
- [9] G. Asrar, M. Fuchs, E. T. Kanemasu, and J. L. Harfield, "Estimating absorbed photosynthetic radiation and leaf area index from spectral reflectance in wheat," *Agron J.*, vol. 76, pp. 300–306, 1984.
- [10] C. J. Tucker and P. J. Sellers, "Satellite remote sensing of primary production," *Int. J. Remote Sens.*, vol. 7, pp. 1395–1416, 1986.
- [11] D. L. Peterson, M. A. Spanner, S. W. Running, and L. Band, "Relationship of Thematic Mapper Simulator data to leaf area index," *Remote Sens. Environ.*, vol. 22, pp. 323–341, 1987.
- [12] S. B. Verma, P. J. Sellers, C. L. Walthall, F. G. Hall, J. Kim, and S. J. Goetz, "Photosynthesis and stomatal conductance related to reflectance on the canopy scale," *Remote Sens. Environ.*, vol. 44, pp. 103–116, 1993.
- [13] R. B. Myneni and D. L. Williams, "On the relationship between FAPAR and NDVI," *Remote Sens. Environ.*, vol. 49, pp. 200–211, 1994.
- [14] J. M. Chen, "Canopy architecture and remote sensing of the fraction of photosynthetically active radiation absorbed by boreal conifer forests," *IEEE Trans. Geosci. Remote Sensing*, vol. 34, pp. 1353–1368, Nov. 1996.
- [15] J. M. Chen and J. Cihlar, "Retrieving leaf area index of boreal conifer forests using landsat TM images," *Remote Sens. Environ.*, vol. 55, pp. 153–162, 1996.
- [16] J. C. Price, "Estimating leaf area index from satellite data," *Remote Sens. Environ.*, vol. 31, pp. 727–734, 1993.
- [17] G. Asrar, R. B. Myneni, and B. J. Choudhury, "Spatial heterogeneity in vegetation canopies and remote sensing of Absorbed Photosynthetically Active Radiation: A modeling study," *Remote Sens. Environ.*, vol. 41, pp. 85–101, 1992.
- [18] G. G. Gutman, "Vegetation indices from AVHRR: An update and future prospects," *Remote Sens. Environ.*, vol. 35, pp. 121–136, 1991.
- [19] N. Gobron, B. Pinty, and M. M. Verstraete, "Theoretical limits to the estimation of the Leaf Area Index on the basis of visible and near-infrared remote sensing data," *IEEE Trans. Geosci. Remote Sensing*, vol. 35, pp. 1438–1445, Nov. 1997.
- [20] M. A. Friedl, F. W. Davis, J. Michaelson, and M. A. Moritz, "Scaling and uncertainty in the relationship between NDVI and land surface biophysical variables: An analysis using a scene simulation model and data from FIFE," *Remote Sens. Environ.*, vol. 54, pp. 233–246, 1995.
- [21] M. A. Friedl, "Examining the effects of sensor resolution and sub-pixel heterogeneity on spectral vegetation indices: Implications for biophysical modeling," in *Scaling of Remote Sensing Data for GIS*, D. A. Quattrochi and M. F. Goodchild, Eds. New York: Lewis, 1996, pp. 113–139.
- [22] C. O. Justice, E. Vermote, J. R. G. Townshend, R. Defries, D. P. Roy, D. K. Hall, V. V. Salomonson, J. L. Privette, G. Riggs, A. Strahler, W. Lucht, R. B. Myneni, Y. Knyazikhin, S. W. Running, R. R. Nemani, Z. Wan, A. R. Huete, W. van Leeuwen, R. E. Wolfe, L. Giglio, J.-P. Muller, P. Lewis, and M. J. Barnsley, "The Moderate Resolution Imaging Spectroradiometer (MODIS): Land remote sensing for global change research," *IEEE Trans. Geosci. Remote Sensing*, vol. 36, pp. 1228–1240, Jul. 1998.
- [23] Y. Zhang, Y. Tian, Y. Knyazikhin, J. V. Martonchik, D. J. Diner, M. Leroy, and R. B. Myneni, "Prototyping of MISR LAI and FPAR and algorithm with POLDER data over Africa," *IEEE Trans. Geosci. Remote Sensing*, vol. 38, pp. 2402–2418, Sept. 2000.
- [24] R. B. Myneni, R. R. Nemani, and S. W. Running, "Estimation of Global Leaf Area Index and Absorbed Par Using Radiative transfer Models," *IEEE Trans. Geosci. Remote Sensing*, vol. 35, pp. 1380–1393, Nov. 1997.
- [25] S. Jacquemond, F. Barret, and J. F. Hanocq, "Modeling spectral and bidirectional soil reflectance," *Remote Sens. Environ.*, vol. 41, pp. 123–132, 1992.
- [26] F. Baret, S. Jacquemond, and J. F. Hanocq, "The soil line concept in remote sensing," *Remote Sens. Rev.*, vol. 7, pp. 65–82, 1993.
- [27] O. Panferov, Y. Knyazikhin, R. B. Myneni, J. Szarzhinski, S. Engwald, K. G. Schnitzler, and G. Gravenhorst, "The role of canopy structure in the spectral variation of transmission and absorption of solar radiation in vegetation canopies," *IEEE Trans. Geosci. Remote Sensing*, to be published.
- [28] A. R. Huete, "A Soil-Adjusted Vegetation Index (SAVI)," *Remote Sens. Environ.*, vol. 25, pp. 295–309, 1988.
- [29] B. Berthelot, G. Dedieu, F. Cabot, and S. Adam, "Estimation of surface reflectances and vegetation index using NOAA/AVHRR: Methods and results at global scale," in *Proc. Commun. 6th Int. Symp. Physical Measurements and Signatures in Remote Sensing*, Val d'Isère, France, Jan. 17–21, 1994.
- [30] B. Berthelot, S. Adam, L. Kergoat, F. Cabot, G. Dedieu, and P. Maisongrande, "A global dataset of surface reflectances and vegetation indices derived from AVHRR/GVI time series for 1989–1990: The LAnd SURface Reflectances (LASUR) data," in *Proc. Commun. 7th Int. Symp. Physical Measurements and Signatures in Remote Sensing*, Courchevel, France, Apr. 7–11, 1997.
- [31] G. Gutman, D. Tarpley, A. Ignatov, and S. Olson, "The enhanced NOAA global land dataset from the Advanced Very High-Resolution Radiometer," *Bull. Amer. Meteorol. Soc.*, vol. 76, pp. 1141–1156, 1995.
- [32] B. N. Holben, "Characteristics of maximum-value composite images from temporal AVHRR data," *Int. J. Remote Sens.*, vol. 7, pp. 1417–1434, 1986.
- [33] P. S. Chavez, Jr., "Radiometric calibration of Landsat Thematic Mapper multispectral images," *Photogramm. Eng. Remote Sensing*, vol. 55, pp. 1285–1294, 1989.
- [34] —, "Image-based atmospheric corrections—Revisited and improved," *Photogramm. Eng. Remote Sensing*, vol. 62, pp. 1025–1036, 1996.
- [35] R. B. Myneni, F. G. Hall, P. J. Sellers, and A. L. Marshak, "The interpretation of spectral vegetation indices," *IEEE Trans. Geosci. Remote Sensing*, vol. 33, pp. 481–486, Mar. 1995.
- [36] J. G. P. W. Clevers, "The application of a weighted infrared-red vegetation index for estimating leaf area index by correcting for soil moisture," *Remote Sens. Environ.*, vol. 29, pp. 25–37, 1989.

Yuhong Tian received the B.S. degree in meteorology from Nanjing Institute of Meteorology, Nanjing, China, in 1992 and the M.S. degree in meteorology from the Chinese Academy of Meteorological Sciences, Beijing, China, in 1995. She is currently pursuing the Ph.D in the Department of Geography, Boston University, Boston, MA, working on prototyping and validating the synergistic algorithm of LAI and FPAR estimation of the MODIS projects.

Her research interests include scale issues in remote sensing and modeling radiative transfer in vegetation canopies.

Yu Zhang received the B.S. degree in physics from the Tsinghua University, Beijing, in 1994 and the M.S. degree in electronics from Peking University, Beijing, China, in 1997. He is currently pursuing the Ph.D. degree in the area of remote sensing and vegetation land surface study in the Department of Geography, Boston University, Boston, MA, working on developing, prototyping, and validating the synergistic algorithm of LAI and FPAR estimation for the MODIS and MISR projects.

His research interests are multi-angle remote sensing and radiative transfer models in vegetation canopies.

Yuri Knyazikhin received the M.S. degree in applied mathematics from Tartu University, Tartu, Estonia, in 1978, and the Ph.D. degree in numerical analysis from the N.I. Muskhelishvili Institute of Computing Mathematics, the Georgian Academy of Sciences, Tbilisi, Georgia, in 1985.

From 1978 to 1990, he was a Research Scientist with the Institute of Astrophysics and Atmospheric Physics and the Computer Center of the Siberian Branch of the Russian Academy of Sciences, Tartu University. He was with the University of Göttingen, Göttingen, Germany, from 1990 to 1996. He is currently a Research Associate Professor, Department of Geography, Boston University, Boston, MA. He has worked and published in areas of numerical integral and differential equations, theory of radiation transfer in atmospheres and plant canopies, remote sensing of the atmosphere and plant canopies, ground-based radiation measurements, forest ecosystem dynamics, and modeling sustainable multifunctional forest management.

Dr. Knyazikhin was an Alexander von Humboldt Fellow from 1992 to 1993.

Ranga B. Myneni received the Ph.D. degree in biology from the University of Antwerp, Antwerp, Belgium, in 1985.

Since 1985, he has been with Kansas State University, Manhattan, the University of Göttingen, Göttingen, Germany, and NASA Goddard Space Flight Center, Greenbelt, MD. He is currently on the Faculty of the Department of Geography, Boston University, Boston, MA. His research interests are in radiative transfer, remote sensing of vegetation, and climate-vegetation dynamics.

Dr. Myneni is a MODIS and MISR science team member.

Joseph M. Glassy received the M.S. degree in forestry from the University of Montana, Missoula, in 1994.

Before pursuing his degree, he was a Programmer/Systems Analyst with Systems for Environmental Management for ten years, designing and implementing biological and Earth science application software with an emphasis on remote sensing, statistical, and spatial analysis. He is currently the Director of Software Development for the Numerical Terradynamics Simulation Group (NTSG), School of Forestry, University of Montana. At the NTSG, he has been the Lead Software Engineer since 1994, developing the NASA Terra platform MODIS land algorithms for FPAR, LAI, PSN, and NPP. His research interests include high performance computer facility design and implementation, scalable systems engineering and software architecture, and developing ecosystem science software at multiple temporal and spatial scales.

Mr. Glassy is a MODIS Team SCF associate.

Gerard Dedieu was born in Carcassonne, France, on May 3, 1956. He received the Ph.D. degree in astronomy, astrophysics, and space techniques from the Paul Sabatier University (UPS), Toulouse, France, in 1984.

In 1988, he joined the Centre National d'Etudes Spatiales (CNES), Toulouse, working as a Research Scientist with Laratoire d'Etudes et de Recherches en Teledetection Spatiale (LERTS), now the Centre d'Etudes Spatiales de la Biosphère (CESBIO), a joint laboratory of CNES-CNRS and UPS. He specialized first in the preprocessing of satellite measurements (atmospheric effect corrections), developing methods to estimate surface parameters (albedo, solar radiation, net primary productivity) and defining data archives for global change studies. From 1993 to 1999, he was in charge of the coordination of the "Terrestrial Biosphere" component of the European Study of Carbon in the Ocean, Biosphere, and Atmosphere (ESCOBA) Project, funded by the European Commission. His main research interests are currently in the development of assimilation techniques of remotely sensed data within regional and global vegetation functioning and SVAT's models. He is also working on the improvement of SPOT 4 vegetation preprocessing techniques and products.

Steven W. Running received the B.S. and M.S. degrees from Oregon State University, Corvallis, and the Ph.D. degree from Colorado State University, Fort Collins.

He was trained as a terrestrial ecologist and has been with the University of Montana, Missoula, since 1979, where he is now a Professor of forestry. His primary research interest is in the development of global and regional ecology by integration of remote sensing with climatology and terrestrial ecology using computer simulation. He is a Member of the Scientific Steering Committee for the Biospheric Aspects of the Hydrologic Cycle Project of the International Geosphere-Biosphere Program. He is also a Team Member for the NASA Earth Observing System, Moderate Resolution Imaging Spectroradiometer (EOS/MODIS).